JOURNAL OF GEOPHYSICAL RESEARCH, VOL. 100, NO. B9, PAGES 17,947–17,963, SEPTEMBER 10, 1995

Strength and rheology of the western U.S. Cordillera

Anthony R. Lowry and Robert B. Smith
Department of Geology and Geophysics, University of Utah, Salt Lake City

Abstract. Effective elastic thickness T_e depends primarily on temperature, composition, and state of stress of the lithosphere. In this paper, we examine high-resolution spectral estimates of T_e and their relationships to regional heat flow, age of the lithosphere, seismic properties, stress orientations, and earthquake focal depths of the western U. S. Cordillera. The relationship of T_e to heat flow indicates that ductile flow accommodates long-term (~10^6 to 10^8 years) isostatic response at different levels of the crust and upper mantle, depending principally on age (and, by implication, bulk composition) of the lithosphere. Isostatic response is primarily controlled by the upper mantle in Archean lithosphere of the middle Rocky Mountains, whereas T_e depends on lower crustal flow in Early Proterozoic lithosphere of the Colorado Plateau. The Yellowstone-Snake River Plain volcanic field and significantly extended regions in the Basin-Range and northern Rocky Mountains are associated with latest Proterozoic aged lithosphere and indicate middle to upper crustal control of long-term T_e. We also show that azimuthal variations of T_e reflect deviatoric stress in the lithosphere. T_e is found empirically to approximate the 95th percentile focal depth of background seismicity. The latter relationship is inconsistent with brittle-ductile control of focal depth, indicating that another rheological transition (e.g., from stick-slip to stable sliding frictional behavior) is responsible. Tectonic and structural relationships expand upon the hypothesis that the geographic distribution of tectonic features depends fundamentally on spatial variations in strength of the lithosphere. Moreover, we find a spatial correlation of the Intermountain Seismic Belt to a marked transition in T_e, implying that forces responsible for this active seismic zone are derived from local buoyancy anomalies rather than from current-day plate boundary interactions.

Introduction

Late Cenozoic extension and seismicity of the western U.S. Cordillera has been, and continues to be, examined in the context of plate interactions [e.g., *Atwater*, 1970], hotspot or plume dynamics [e.g., *Smith and Sbar*, 1974], and gravitational potential energy stored during Late Cretaceous/early Tertiary contraction [e.g., *Wernicke et al.*, 1987]. Tectonic models derived from these mechanisms have been used to explain the observed temporal and spatial distributions of extension and volcanism, but the relative importance of each process has yet to be defined. It is expected that a working model of Cordilleran extension should incorporate an understanding of both the three-dimensional rheological response of continental lithosphere and the relative importance of forces acting upon it. However, force balances and rheology of continental lithosphere are poorly resolved at this time.

An important component of rheological response is the resistance to bending by the Earth's elastic layer. Bending strength of the lithosphere is characterized by its flexural rigidity, or equivalently, effective elastic thickness T_e. A maximum entropy-based approach to coherence analysis of topography and gravity fields [*Lowry and Smith*, 1994] maps long-term (~10^6 to 10^8 years) T_e at scales of individual tectonostratigraphic features. We apply this approach to the western U.S. Cordillera, focusing on the 1300-km-long, north-south trending Intermountain Seismic Belt (ISB). The ISB is a ~100–200 km wide zone of intraplate seismicity with shallow focal depths, generally < 20 km deep, that coincides with the eastern margin of late Cenozoic extensional deformation of the western United States [*Smith and Sbar*, 1974; *Smith and Arabasz*, 1991]. Contemporary strain across the ISB inferred from cumulative moments of historic earthquakes [*Eddington et al.*, 1987] and terrestrial and satellite-based geodetic surveys [*Martinez et al.*, 1994] comprises about half the total ~1 cm/yr Basin-Range opening rate indicated by satellite geodesy and geologic constraints [e.g., *Minster and Jordan*, 1987; *DeMets et al.*, 1987; *Dixon et al.*, 1995].

Paper number 95JB00747
0148-0227/95/95JB-00747$05.00

Effective elastic thickness is an integral function of temperature, composition, and state of stress of the lithosphere. Consequently, T_e has provided important insight into rheology and state of stress for oceanic lithosphere [e.g., *Goetze and Evans*, 1979; *McNutt and Menard*, 1982]. Rheological studies of continental lithosphere generally have not incorporated T_e, however, partly because of the greater complexity of temperature and compositional variations in continents, and partly because of an inability to resolve T_e at the scale of individual tectonic features. However, recent improvements in the resolution of T_e estimates [*Lowry and Smith*, 1994] permit preliminary assessment of the relationship of T_e to rheology and state of stress. For example, the depth at which ductile flow accommodates isostatic response can be seen to exhibit a strong dependence on age of the lithosphere. An apparent relationship of azimuthal variations in T_e to lithospheric stress is also explored, and the relationship of T_e to maximum seismogenic depth in the crust confirms that depth of background seismicity is not defined by the rheological transition from frictional slip to dislocation creep.

The results of this analysis are insufficient to argue for a particular model of extension. However, focusing of seismic activity along zones of transitional strength suggests that forces responsible for contemporary extension and seismicity of the eastern Basin-Range do not originate at great distance, so modern plate boundary interactions are not likely to be directly involved. We suggest instead that extensional stresses responsible for the ISB are derived from local variations in lithospheric buoyancy (as defined by density averaged over the thickness of the lithosphere).

Determination of Elastic Thickness

Effective elastic thickness T_e is a conceptual representation of the flexural rigidity, or resistance to bending, D, of the lithosphere. T_e approximates the Earth's uppermost, elastically deforming layer as a perfectly elastic, thin plate, in which case

$$T_e = \left[\frac{12\left(1-\nu^2\right)D}{E}\right]^{1/3}, \tag{1}$$

where ν is Poisson's ratio and E is Young's modulus of the material [e.g., *Turcotte and Schubert*, 1982]. It is important to note that T_e is not a physical length parameter but an alternative expression of bending strength. T_e invariably underestimates the true thickness of the elastically deforming layer because it does not account for anelastic failure, and it can differ from the true thickness by more than 100% [e.g., *McNutt and Menard*, 1982].

T_e is estimated from observations of the Earth's response to loading. Compensation of short-wavelength loads is distributed by the strength of an elastic plate, whereas long-wavelength loads have a larger component of local compensation. The degree to which compensation is localized versus regionally distributed depends on the flexural rigidity. Thus one can solve for the loads and the load response, hence T_e, from comparison of topography or bathymetry to gravitational potential in the form of a free air, Bouguer or geoid anomaly field. A maximum entropy-based analysis of coherence of topography and Bouguer gravity, as described by *Lowry and Smith* [1994], is used in this paper. This approach enables systematic mapping of T_e with resolution approaching the scale of tectonostratigraphic features mapped at the surface. Comparison of our estimates of T_e with heat flow, geologic information, and independent determinations of elastic thickness indicates that coherence analysis can be used to reliably map T_e at scales of less than 100 km [*Lowry and Smith*, 1994].

Coherence analysis was applied to the companion topography and complete Bouguer gravity data used by *Simpson et al.* [1986] to develop an isostatic residual gravity map of the United States. Gravity data are gridded at a 4-km spacing from similarly distributed measurements that were processed to remove outliers [*O'Hara and Lyons*, 1983]. The topographic data are on an identical grid generated specifically for tandem signal processing [*Simpson et al.*, 1986]. Flexural rigidity was estimated for 200 km by 200 km and 400 km by 400 km windows of the data, with centers spaced at 50-km intervals. Rigidity estimates were then interpolated to a 10-km spacing using a minimum curvature algorithm. The close spacing requires significant overlap of data windows for neighboring estimates of flexural rigidity, implying some smoothing of the rigidity distribution. Flexural rigidity was converted to T_e assuming a Young's modulus of 10^{11} Pa and Poisson's ratio of 0.25. Variations of density with depth were constrained using published crustal seismic velocity data from the Cordillera, detailed in Table 1.

Elastic Thickness of the Western U.S. Cordillera

Previous investigations of continental T_e have concluded that (1) greater T_e generally corresponds to greater age of lithospheric genesis [*Bechtel et al.*, 1990] and lower heat flow [*Lowry and Smith*, 1994]; (2) significant extension is limited to domains of low T_e [*Lowry and Smith*, 1994]; and (3) thin skin contractional deformation fronts generally occur 50 to 200 km toward the higher strength side of transitional zones of T_e [*Lyon-Caen and Molnar*, 1983]. These observations are reinforced by results presented in Plate 1, and by comparison with Figure 1. Also, a striking correlation occurs between epicenters defining the ISB and the east to west transition from high to low T_e (Plate 1a).

A summary of Cordilleran T_e, along with other pertinent information, is given by physiographic province in Table 2. The volcanic provinces, including the eastern and western Snake River Plain and the margins of the Columbia Basin, have the lowest T_e, ~6 km (Plate 1; Table 2). Notably, however, the interior of the Columbia Basin is much stronger, $T_e \approx$ 19 km. Outside of the volcanic provinces, the next-lowest T_e, ~9 km, occurs in the northern Basin-Range and northern Rocky Mountains provinces, where significant late Cenozoic extension has occurred. Strongly extended domains, such as are described by *Wernicke* [1991], exhibit the lowest T_e in the extensional provinces. There are pockets of higher T_e within these two provinces, however; one such area in the north-central Basin-Range coincides with an older isotopic domain described by *Farmer and DePaolo* [1983] (Plate 1a). T_e of the Early Proterozoic Colorado Plateau, ~22 km, is significantly higher than the Late Proterozoic-aged lithosphere further west. The highest T_e, averaging 30 km, occurs in the Archean middle Rocky Mountains.

Parameterization of T_e

Correlations of T_e to the various manifestations of tectonism are intriguing, but we can greatly improve our understanding of the rheological implications of T_e with a simple, conceptual analysis of yield strength. T_e ultimately depends on the bending stresses maintained by the lithosphere, which in turn depend on the failure properties of rock. Depth dependent failure is commonly approximated via a yield strength envelope [*Goetze and Evans*, 1979] defined by the lesser of the sustainable differential stresses, $\Delta\sigma$, governed by frictional resistance and dislocation creep. We adopt the linear frictional failure relations:

$$\Delta\sigma = \left[\left(\sqrt{\mu^2+1}-\mu\right)^{-2}-1\right]\rho g z\left(1-\lambda\right), \tag{2}$$

to describe a compressional stress regime and

$$\Delta\sigma = \left[1-\left(\sqrt{\mu^2+1}-\mu\right)^{2}\right]\rho g z\left(1-\lambda\right), \tag{3}$$

Table 1. Velocity and Density Values Used to Constrain the Inversion

	Easternmost Basin and Range[a]			Western Middle Rocky Mountains[a]		
Layer	Depth to Top, km	*P* Velocity, km/s	Density, kg/m³	Depth to Top, km	*P* Velocity, km/s	Density, kg/m³
1	0	3.4	2280	0	4.6	2470
2	2	6.0	2700	3	5.9	2680
3	8	5.5	2610	16	6.7	2870
4	15	6.5	2800	40	7.9	3230
5	25	7.4	3050	--	--	--

	Eastern Snake River Plain[b]			Colorado Plateau[c]		
Layer	Depth to Top, km	*P* Velocity, km/s	Density, kg/m³	Depth to Top, km	*P* Velocity, km/s	Density, kg/m³
1	0	3.3	2270	0	3.0	2210
2	2	5.2	2560	2	6.2	2740
3	5	6.1	2730	26	6.8	2880
4	11	6.5	2810	41	7.8	3190
5	19	6.8	2880	--	--	--
6	42	7.9	3240	--	--	--

	East-Central Basin-Range[d]			Northern Rocky Mountains[e]		
Layer	Depth to Top, km	*P* Velocity, km/s	Density, kg/m³	Depth to Top, km	*P* Velocity, km/s	Density, kg/m³
1	0	3.0	2210	0	4.5	2460
2	2	5.9	2680	2	6.2	2730
3	13	6.4	2790	18	6.8	2880
4	27	7.4	3070	33	8.0	3280

	Yellowstone Plateau[f]			Great Plains[g]		
Layer	Depth to Top, km	*P* Velocity, km/s	Density, kg/m³	Depth to Top, km	*P* Velocity, km/s	Density, kg/m³
1	0	2.8	2170	0	3.8	2360
2	1	5.7	2650	15	6.0	2700
3	15	6.7	2860	23	7.4	3060
4	43	7.9	3240	33	8.2	3370

	Northwestern Basin-Range[h]			Western Snake River Plain[i]		
Layer	Depth to Top, km	*P* Velocity, km/s	Density, kg/m³	Depth to Top, km	*P* Velocity, km/s	Density, kg/m³
1	0	2.8	2170	0	2.0	1960
2	1	5.6	2630	2	5.2	2560
3	6	6.1	2710	10	6.7	2850
4	19	6.4	2780	42	7.9	3230
5	31	8.0	3270	--	--	--

[a] *Braile et al.* [1974].
[b] *Braile et al.* [1982].
[c] *Roller* [1965].
[d] *Mueller and Landisman* [1971].
[e] *Sheriff and Stickney* [1984] and *Sparlin et al.* [1982].
[f] *Lehman et al.* [1982].
[g] *McCamy and Meyer* [1964].
[h] *Benz et al.* [1990].
[i] *Hill and Pakiser* [1966].

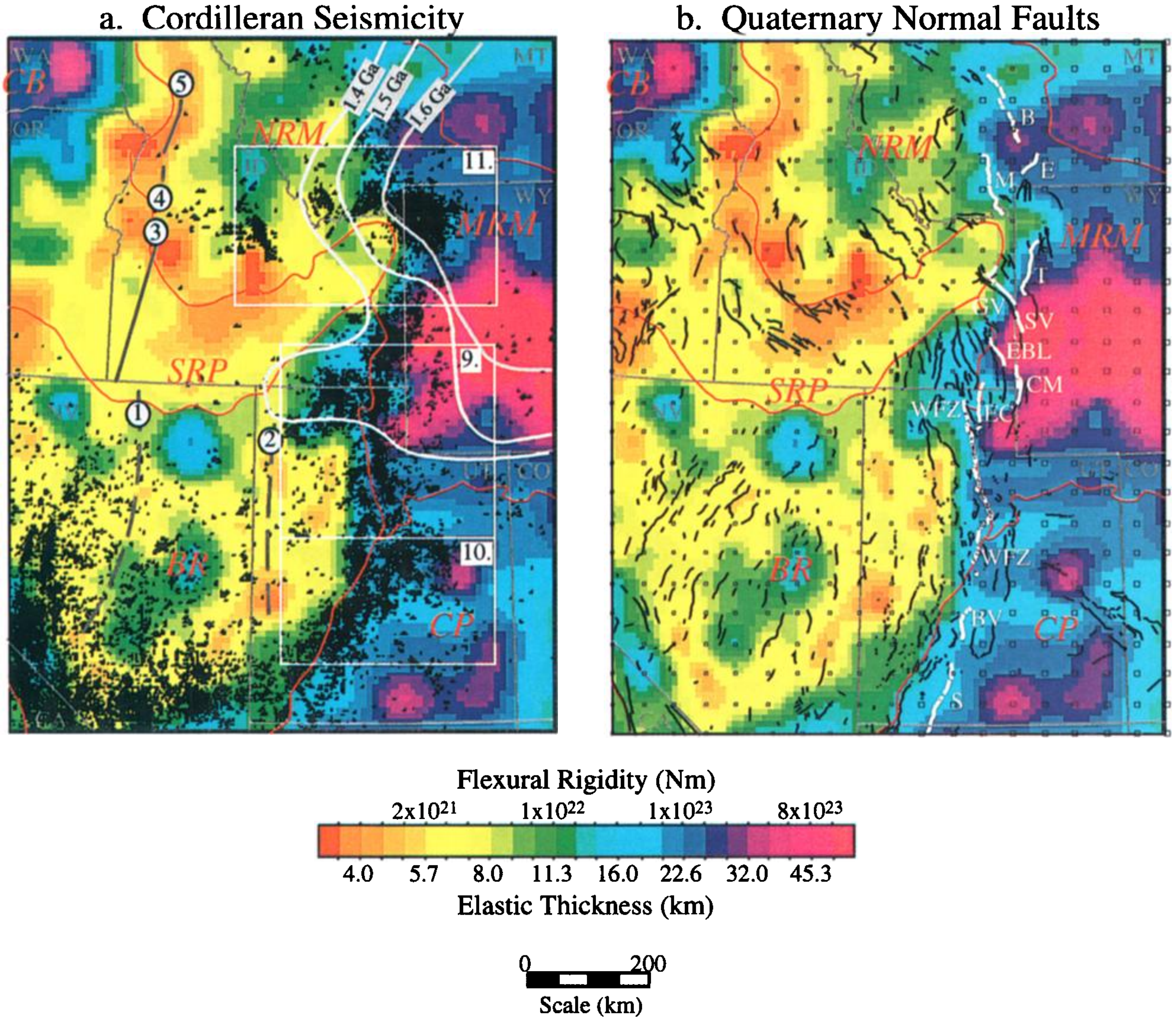

Plate 1. Elastic thickness of the western U.S. Cordillera, with historic seismicity and Cenozoic normal faults. (a) Earthquake epicenters, $M_L > 1$, recorded by University of Utah, University of Nevada-Reno, and U.S. Geological Survey seismograph networks. The white boxes locate ISB seismicity examined in detail in Figures 9, 10, and 11. Light grey lines are K/Ar isotopic ages of the Archean Wyoming craton [*Condie*, 1981]. Darker grey lines are boundaries between genetically distinct lithospheric blocks located via geochemistry of magmas, from (1) and (2) *Farmer and DePaolo* [1983], (3) *Leeman et al.* [1992], (4) *Manduca et al.* [1992], and (5) *Fleck and Criss* [1985]. (b) Surface traces of normal faults exhibiting late Quaternary (<500 ka) surface rupture [after *Hecker*, 1993; *Smith and Arabasz*, 1991]. Thick white lines are the easternmost faults with significant, > 1 km, offset. Faults are B, Bozeman; BV, Beaver; CM, Crawford Mtns; E, Emigrant; EBL, East Bear Lake; EC, East Cache; GV, Grand Valley; M, Madison; S, Sevier; SV, Star Valley; T, Teton; WFZ, Wasatch Fault Zone. Boxes indicate locations of T_e estimates (larger boxes are 400 km by 400 km windows; smaller are 200 km by 200 km windows of data). Physiographic provinces are BR, Basin-Range; CB, Columbia Basin; CP, Colorado Plateau; MRM, middle Rocky Mountains; NRM, northern Rocky Mountains; SRP, Snake River Plain.

for extension, where μ is the coefficient of static friction, ρ is density of overburden, g is acceleration of gravity, z is depth, $\lambda = P/\rho g z$, and P is pore pressure [e.g., *Sibson*, 1974]. Power law creep is described by

$$\Delta\sigma = \left(\frac{\dot{\varepsilon}}{A}\right)^{1/n} \exp\left(\frac{H^*}{nRT}\right) \qquad (4)$$

where $\dot{\varepsilon}$ is strain rate, A and n are empirically derived material constants, R is the gas constant, T is temperature, and H^* is the activation energy of the material [e.g., *Goetze and Evans*, 1979]. A more sophisticated estimate of yield strength might also incorporate contributions from the low-temperature ductile and semibrittle rheological regimes, but frictional slip and ductile creep are generally sufficient for flexural analysis [*McNutt and Menard*, 1982].

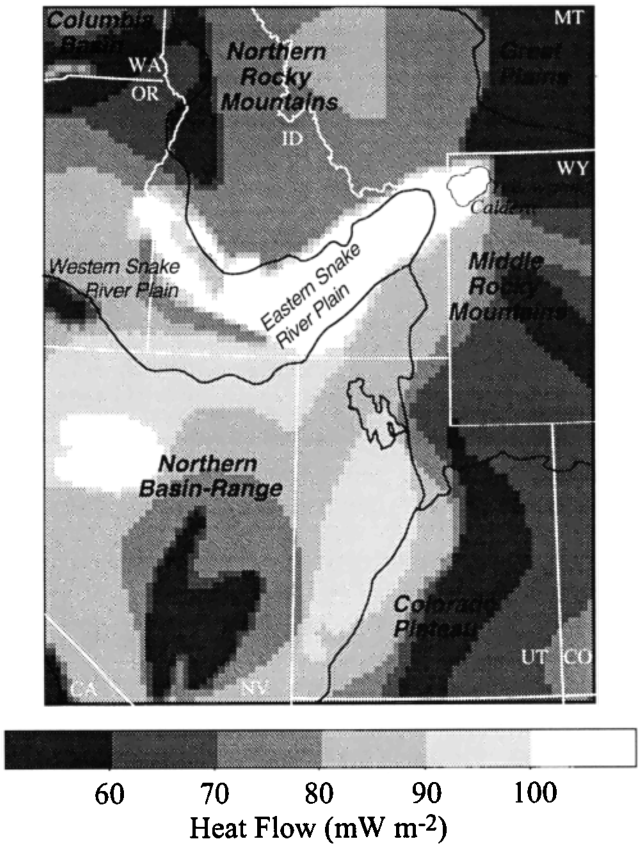

Figure 1. Regional surface heat flow [after *Blackwell and Steele*, 1992].

Examples of yield strength envelopes for continental crustal materials are given in Figure 2a. Corresponding flow law parameters are listed in Table 3. Envelopes are also shown for a range of continental geothermal gradients (Figure 2b). Note that, because the power law creep relation approaches but never equals zero differential stress, envelopes are truncated at a small differential stress value (in this paper, $\Delta\sigma$ = 40 MPa) chosen such that the contribution to T_e from greater depths is negligible [*McNutt*, 1984]. It is readily apparent that yield strength profiles can vary significantly with temperature field and bulk composition at depths of ductile creep.

The state of stress relative to rock strength is also important. Flexural rigidity depends on plate bending moment M via

$$D = -\frac{M}{K} \tag{5}$$

where K is the curvature of the plate [e.g., *Turcotte and Schubert*, 1982]. The moment in turn corresponds to the vertically integrated fiber stress σ_f generated by bending, weighted by distance from a neutral surface at depth z_n (see Figure 3a):

$$M = \int_0^{T_m} \sigma_f(z)\,(z - z_n)\,dz, \tag{6}$$

where T_m is mechanical thickness of the plate (i.e., that sup-

Table 2. Summary of Lithospheric Properties and Other Pertinent Information, by Physiographic Province

Province	Average Elevation, m	Average Heat Flow,[a] mW m^{-2}	Lithospheric Age, Ga	Crustal Thickness,[b] km	P_n Velocity, km s^{-1}	Average Elastic Thickness,[c] km	Range of T_e,[c] km	Primary Depth of Accommodation[c]
Snake River Plain and Columbia Basin Margin	1420	100	0.6[d]	40	7.9	6	3.2 – 9.4	middle to upper crust
Northern Rocky Mountains	1680	75	0.6[d,e]	40 – 45[f]	7.9 – 8.1	8	3.8 – 16	middle to upper crust
Northern Basin-Range	1610	85	0.6[d,e]	30 – 35	7.7 – 7.8	9	4.1 – 19	middle to upper crust
Interior Columbia Basin	940	70	unknown	40	8.0 – 8.1	19	7.2 – 49	lower crust
Colorado Plateau	1980	70	1.8[g]	40	7.8	22	12 – 37	lower crust
Middle Rocky Mountains	2170	70	> 2.5[h]	40 – 45	7.9 – 8.0	30	10 – 77	mantle

[a]after *Blackwell and Steele* [1992].
[b]after *Braile et al.* [1989].
[c]This study.
[d]*Armin and Mayer* [1983] and *Bond and Kominz* [1984].
[e]Parts of the Basin-Range and northern Rocky Mountains are older (see text).
[f]*Sheriff and Stickney* [1984] indicate 33 km for northern Rocky Mountains; that would be more consistent with other data.
[g]*DePaolo* [1981].
[h]*Condie* [1981].

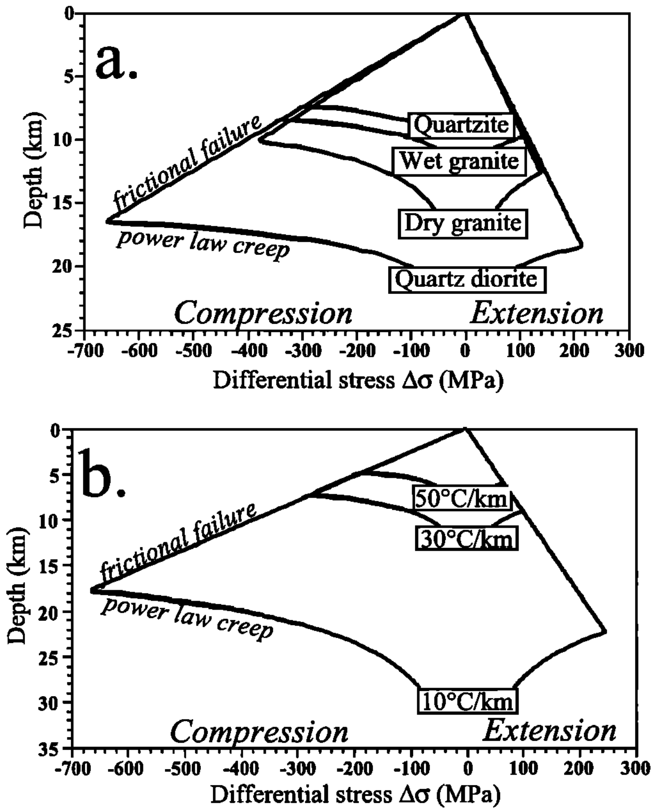

Figure 2. Yield strength envelopes (a) for various crustal rheologies, assuming a geothermal gradient of 20°C km^{-1} and a strain rate of 10^{-15} s^{1}; and (b) for various geothermal gradients, using a dry-granite rheology and 10^{-15} s^{-1} strain rate.

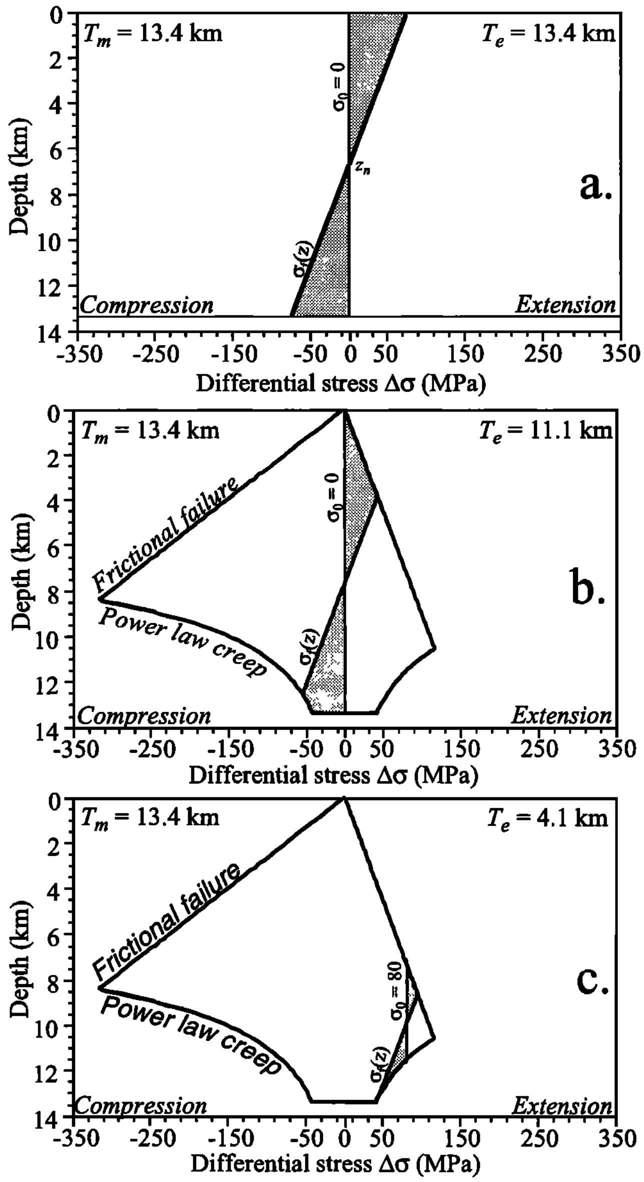

Figure 3. Fiber stresses in a thin bending plate. T_e depends on bending moment, i.e., integral of the shaded area weighted by distance from the neutral surface z_n. (a) For a perfectly elastic plate, mechanical thickness T_m equals elastic thickness T_e. (b) If yield strength is limited by frictional slip and ductile creep, sustainable bending moment, and hence T_e, is decreased. (c) Bending moment is decreased further by superimposition of a large tectonic stress. Envelopes are for dry granite with temperature gradient 25°C km^{-1} and strain rate 10^{-15} s^{-1}.

ports deviatoric stress on geologic timescales). In a thin, perfectly elastic plate, the fiber stress varies according to

$$\sigma_f = -\left(\frac{E}{1-\nu^2}\right) K (z - z_n). \tag{7}$$

Superimposing a yield strength limit truncates the plate bending stresses (Figure 3b) so that bending moment, and consequently the effective elastic thickness, is reduced, i.e., $T_e < T_m$ [*McNutt and Menard*, 1982]. Figure 4a illustrates the effect of increasing plate curvature on T_e. A uniform, regional horizontal stress (henceforth in this paper referred to as a "tectonic" stress) will also have significant effect on T_e [*McNutt*

Table 3. Material Parameters Used in This Study

Rock Composition	Density ρ, kg m^{-3}	Young's Modulus E, Pa	Power Law Coefficient A, MPa^{-n} s^{-1}	Power Law Exponent n	Activation Energy H^*, kJ mol^{-1}	Thermal Conductivity K, W m^{-1} °K^{-1}
Dry granite	2600	7×10^{10}	2.5×10^{-9}	3.4	139.	2.4–3.8
Wet granite	2600	7×10^{10}	2.0×10^{-4}	1.9	137.	2.4–3.8
Dry quartzite	2600	7×10^{10}	3.2×10^{-5}	1.9	123.	4.2–6.3
Diorite	2700	7×10^{10}	1.3×10^{-3}	2.4	219.	2.6–3.5
Dry olivine	3250	8×10^{10}	6.3×10^{4}	3.5	533.	3.7–4.6

Power law properties are from *Hansen and Carter* [1982] for crustal compositions and from *Kirby* [1983] for olivine.

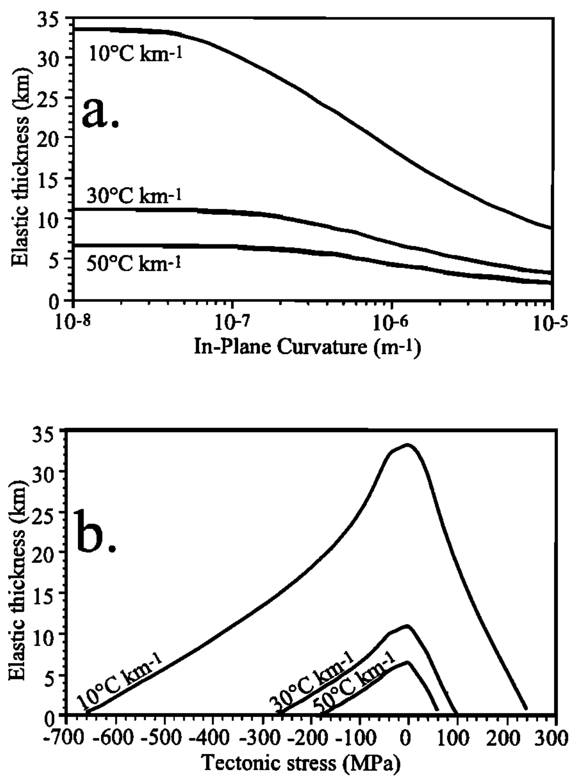

Figure 4. Dependence of elastic thickness on state of stress for a dry-granite composition, strain rate of 10^{-15} s^{-1}, and various geothermal gradients. (a) T_e versus fiber stress (expressed as plate bending curvature), assuming no far-field stress, and (b) T_e versus tectonic stress, given small curvature, 10^{-8} m^{-1}.

and Menard, 1982]. A superimposed tectonic stress σ_0 will shift the reference axis, $\sigma_f(z) = 0$, within the yield strength envelope as indicated in Figure 3c. As the reference state of stress moves outward to either limb of the envelope, the sustainable bending moment (and hence T_e) is decreased. T_e as a function of superimposed tectonic stress is shown in Figure 4b.

T_e and Tectonics

Parameter Sensitivity of T_e

From inspection of equations (1) through (7), T_e depends upon the elastic properties of rock; the coefficient of friction and pore fluid pressure at depths of frictional failure; composition, strain rate and temperature at ductile depths; and the state of stress due to plate bending and tectonic forces. Many of these properties are poorly constrained for most continental lithosphere; that combined with the sheer number of variables makes analysis of the implications of T_e a somewhat daunting task. However, T_e is much more sensitive to some parameters than to others. Figure 5 displays the sensitivity of T_e to reasonable ranges of each of its variable parameters, as well as a typical range of standard error for estimates of T_e from the Basin-Range (calculated from the method described by *Lowry and Smith* [1994]). Virtually all of the sensitivities scale logarithmically, such that if a different reference state were chosen, the sensitivity ranges would be displaced on the log plot, but lengths of the bars would remain approximately the same. (The exceptions are for μ and λ, which would show decreased sensitivity ranges given a less extreme state of lithospheric stress.) Thermal gradient, state of stress (due to plate bending and tectonic loading), and power law composition are the only parameters whose sensitivity ranges are significant when

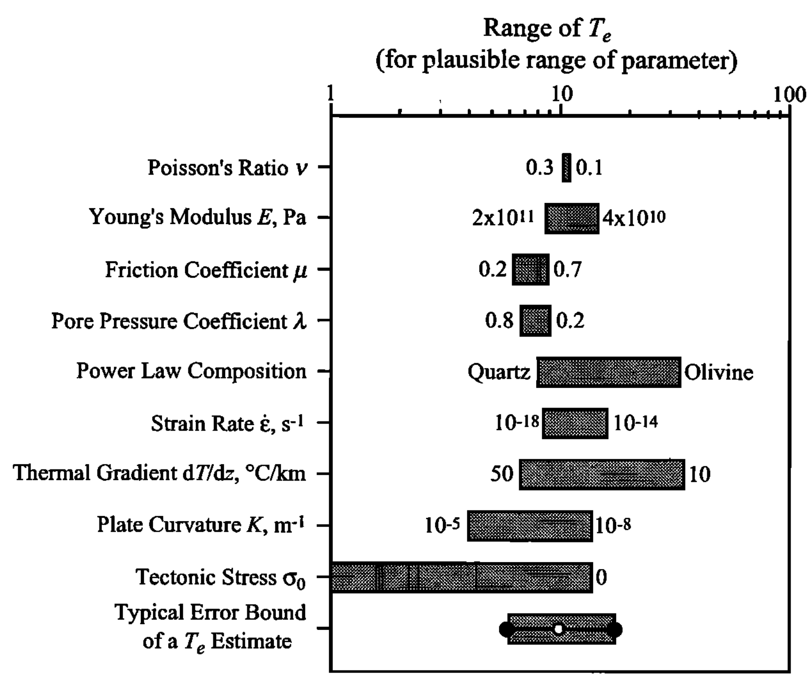

Figure 5. Sensitivity of T_e to its variable parameters. Ranges for ν and E are for $D = 10^{22}$ N m; μ and λ sensitivities use an extreme plate curvature $K = 10^{-6}$ m^{-1}; all other cases use dry granite rheology with $\sigma_0 = 0$, $K = 10^{-8}$ m^{-1}, $dT/dz = 25$°C km^{-1}, $\dot{\varepsilon} = 10^{-15}$ s^{-1}, $\lambda = 0.37$ and $\mu = 0.65$, except as otherwise indicated. Error bounds for a typical T_e estimate are included for comparison. Power law rheology, thermal gradient, and state of stress have the most significant effects on T_e.

compared to the range of error in T_e. T_e error ranges also scale logarithmically, and are more a reflection of resolution than of random error: T_e estimation assumes uniform and isotropic rigidity within a data window, whereas actual strength properties can vary dramatically (e.g., Plate 1a) and also vary with direction. In general, a factor of 2 change can be considered significant relative to the resolution of T_e estimates [e.g., *Bechtel et al.*, 1990].

Parameters that have insignificant influence on T_e are fixed for the remainder of this discussion. We adopt previous convention [e.g., *Brace and Kohlstedt*, 1980] by using $\mu = 0.65$ and $\lambda = 0.37$. Some studies suggest that dynamic shear stress on major faults is a factor of 3 to 10 lower than predicted by these parameters [*Zoback et al.*, 1987; *Bird and Kong*, 1994], but changing the linear friction coefficients to reflect these studies would have no impact on this analysis. We assume strain rates are depth-independent and range from 10^{-18} to 10^{-14} s^{-1}, as inferred from geodetic measurements and cumulative moments of historic earthquakes [*Eddington et al.*, 1987; *Dzurisin et al.*, 1990; *Savage et al.*, 1992; *Martinez et al.*, 1994].

The three most important properties in defining T_e, temperature, power law composition, and state of stress, can all be constrained to some extent from independent data. Regional heat flow patterns [e.g., *Blackwell et al.*, 1991] provide insight into the temperature field. Seismic velocity structure [e.g., *Braile et al.*, 1989] can be used to infer composition [e.g., *Fountain and Christensen*, 1989]. Stress magnitudes at depths of interest are not known, but aspects of the state of stress can be inferred from principal stress directions given by stress measurements and stress indicators [e.g., *Zoback and Zoback*, 1989], and from the maximum depths of frictional failure observed in earthquakes.

Heat Flow

Sensitivity of T_e to thermal gradient is reflected in the strong correlation between areas of low T_e (Plate 1) and high heat flow (Figure 1). Regional heat flow Q, digitized from *Blackwell and Steele* [1992], is plotted against measurements of T_e in Figure 6. Linear regression of Q versus T_e yields a negative slope to > 99% confidence, but with a correlation coefficient of –0.46 and very significant variance. Some of the scatter can be attributed to the poor resolution of T_e estimates as well as the poor distribution of, and influence of hydrology on, Q measurements, but part of the scatter occurs because T_e depends on other factors besides just temperature. The predictive relationship between heat flow and T_e, from equations (1) through (7), is also shown in Figure 6 for several crustal and upper mantle rock types, using a geothermal gradient estimated from $dT/dz = Q/\kappa$, where κ is thermal conductivity. Clearly, the regression relationship is inconsistent with a power law corresponding to a single, uniform composition.

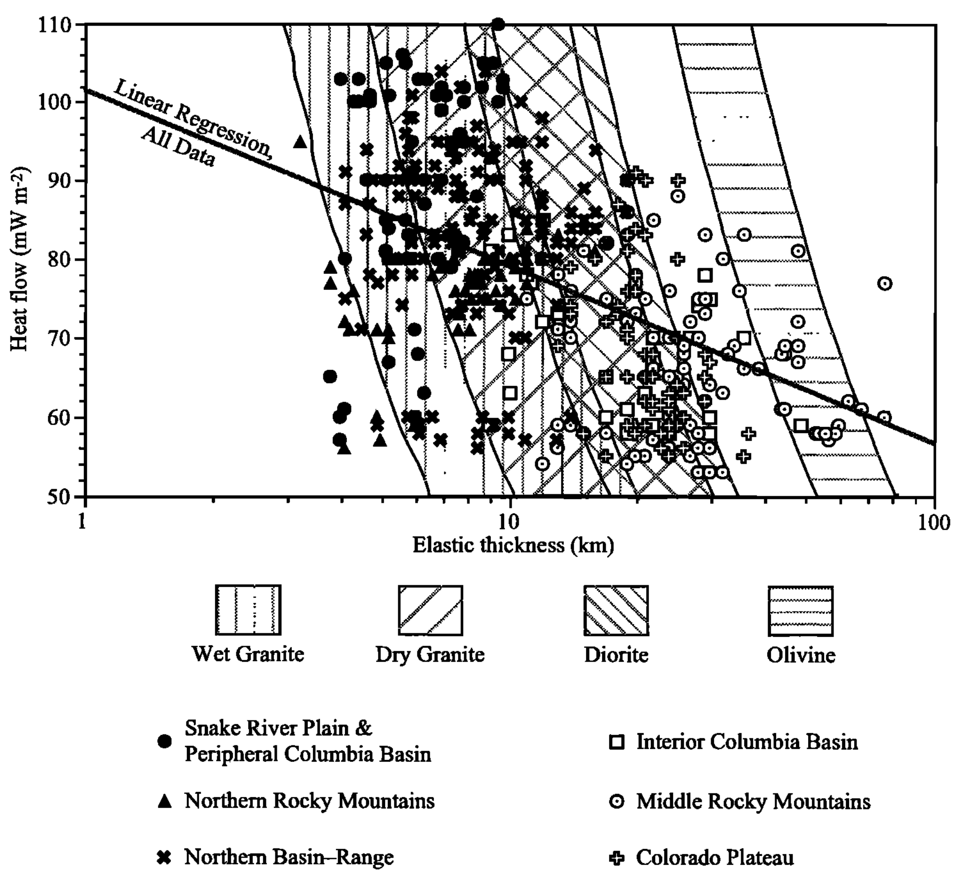

Figure 6. Regional heat flow, digitized from *Blackwell and Steele* [1992], versus estimates of T_e. Locations of T_e estimates are indicated by province. The predictive range for various compositions, indicated by light grey cross-hatch, is based on the range of thermal conductivity (Table 3) and strain rates ranging from 10^{-14} to 10^{-18} s^{-1}.

Compositional Control of T_e

The particular power law that defines T_e depends primarily on thermal gradient and compositional layering of the lithosphere. In general, higher thermal gradients should mobilize rocks in shallower rheological layers. We have noted that T_e tends to be relatively consistent within physiographic provinces, but can vary dramatically from one province to another (Plate 1a; Table 2), and so one might reason that different provinces are characterized by activation of different rheological layers as a result of variations in mantle heat flow. Then the relationship of T_e to Q should be more consistent with the relationship predicted for a single uniform composition if the observations are broken out by province. This is indeed the case (see Figure 6). T_e versus Q of the Colorado Plateau hovers near the quartz diorite (~lower crustal) predictive relationship. The relationship in the middle Rocky Mountains is most consistent with lower crustal and mantle rheological control. Results from the Basin-Range, northern Rocky Mountains, and the volcanic provinces mostly fall within the range of upper to middle crustal (quartzo-feldspathic) rheology, except for the interior Columbia Basin, which is more consistent with a lower crustal relationship.

There remains an obvious problem, however, in that each of the physiographic provinces spans nearly the same range of heat flow. If thermal gradient alone determines the rheological layer that responds with ductile flow, then heat flow should break out according to province as well as T_e. There are a couple of reasons why it does not: (1) the regional heat flow interpreted by *Blackwell and Steele* [1992] is sensitive to near-surface processes that are independent of mantle heat flow (for example, the < 60 mW m^{-2} anomaly in the central Basin-Range (see Figure 1) is thought to have a hydrologic origin), and (2) the defining rheology also depends on bulk composition of the layers.

Jordan [1978, 1981] notes that compositional differentiation to depths of > 200 km is necessary to account for the buoyancy, petrology and seismic velocity structure of continental mantle. According to his hypothesis, cratonic lithosphere is stabilized by depletion of mantle basalt during extreme tectonomagmatic events, resulting in reduced density, viscosity, and thermal conductivity; Archean lithosphere tends to be most stable because it has experienced the most cycles of tectonomagmatic fractionation [*Jordan*, 1981]. Correlation of high T_e with greater lithospheric age (Table 2) is consistent with a bulk compositional influence on rheology, and compositional stabilization also helps to explain the apparent long-term persistence of lithospheric strength variations [*Lowry and Smith*, 1994]. However, whereas *Jordan*'s [1981] stabilization hypothesis focuses on the chemistry of mantle rocks, the rheology of many western U.S. provinces is controlled by crustal compositions. Hence the uniformity of T_e within provinces having uniform ages but varying heat flow would suggest that tectonomagmatic fractionation may increase the relative stability of crustal layers as well as the mantle.

The power law compositions implicit in Figure 6 are supported by comparison of T_e with depth to seismic velocity discontinuities detailed in Table 1. For example, T_e of much of the middle Rocky Mountains approaches or exceeds the ~40 km thickness of the crust. Given that T_e underestimates T_m, flexural strength must be controlled by the upper mantle. T_e in the Basin-Range, Snake River Plain, and northern Rocky Mountains is much less than crustal thickness, and averages less than half the depth to the base of the midcrust, generally ~15 to 20 km. Thus a middle to upper crustal power law composition is a reasonable assumption. Colorado Plateau T_e averages 22 km, and crustal thickness is 35 to 45 km, whereas depth to top of the lower crust is about 25 km. Hence, assuming moderate reduction of elastic thickness by stress, a lower crustal control of T_e would be most probable.

Stress Orientations and Anisotropy of T_e

Figure 4 represents the reduction of T_e by stress when horizontal components of the principal stress tensor, $\sigma_{h\max}$ and $\sigma_{h\min}$, are equal. One can infer, however, that if $\sigma_{h\max}$ is significantly greater than $\sigma_{h\min}$, there should be an azimuthal variation in T_e. Examples in Figures 7a, 7b, and 7c show the azimuthal dependence of T_e predicted by application of equations (1) through (7) to examples of extensional, strike-slip, and compressional tectonic stress regimes.

Observations of lithospheric state of stress are generally limited to indicators of principal stress directions, including stress inversions of fault slip data and focal mechanisms [*Angelier*, 1984; *Gephart and Forsyth*, 1984], well bore breakouts [*Gough and Bell*, 1981], and volcanic vent alignments [*Nakamura*, 1977]. In situ measurements such as hydraulic fracturing [*Hickman and Zoback*, 1983] and overcoring [*McGarr and Gay*, 1978] provide stress magnitudes, but only in the upper few kilometers of the crust. However, the effect of stress on isostatic response can be qualitatively evaluated by comparison to stress orientations. Figure 7d is an example of observed azimuthal variation of T_e from the eastern Snake River Plain. Formal mathematical inversion for axes of a best fitting ellipse yields a minor axis direction of N49°E±13°. Thus, assuming the anisotropy reflects a state of extensional deviatoric stress, the N49°E direction should correspond to $\sigma_{h\min}$. Volcanic vent alignments at the same location indicate an extensional state of stress with minimum compression direction N48°E [*Zoback and Zoback*, 1989].

Bechtel [1989] notes anisotropy of T_e in both the Basin-Range and East African Rift extensional provinces that he attributes to mechanical weakening of the elastic layer by faults. However, we observe as much as 50% reduction of T_e in the minor axis direction, which is too large to account for by alignment of faulting. Frictional slip can occur for a broad range of fracture orientations with relatively minor variation in frictional yield strength [e.g., *Forsyth*, 1992], and we observe minor axis directions of T_e in the middle Rocky Mountains and elsewhere that are not perpendicular to nearby faults. Hence it is probably more accurate to associate anisotropy of T_e with stress orientation than with fault orientation.

Figure 7 indicates a different pattern for each of the three stress regimes, but the patterns are not diagnostic. For example, the bilobate pattern in the extensional example (Figure 7a) might be observed in a compressional stress regime if $\sigma_{h\max} - \sigma_v$ approaches the maximum yield strength of the lithosphere. It could also be seen in a region of strike-slip if one horizontal principal stress were near the lithostat, σ_v. The only diagnostic pattern is the cloverleaf pattern of Figure 7b, predicted only for strike-slip stress. Hence if azimuthal variation of T_e is to be used to infer principal stress orientation, independent information about the stress regime (focal mechanisms, for example) will be needed to determine whether the

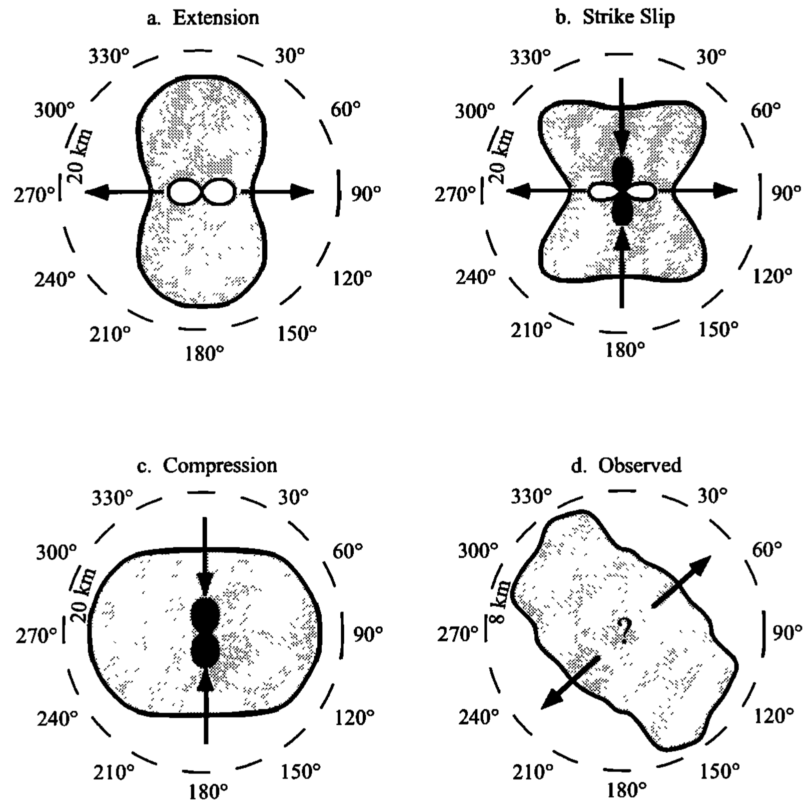

Figure 7. Examples of azimuthal variation of T_e. Figures 7a, 7b, and 7c were modeled using a dry-granite power law rheology, strain rate of 10^{-15} s^{-1} and 20°C km^{-1} geothermal gradient. Arrows indicate horizontal principal stress directions; smaller patterns are tectonic stress σ_0 in (black fill) compression, or (white fill) extension. (a) Deviatoric extension, with $\sigma_{h\max} = \sigma_v$ and $\sigma_{h\min} = \sigma_v + 80$ MPa. (b) A strike-slip stress regime, with $\sigma_{h\max} = \sigma_v - 80$ MPa and $\sigma_{h\min} = \sigma_v + 80$ MPa. (c) Deviatoric compression, with $\sigma_{h\max} = \sigma_v - 80$ MPa and $\sigma_{h\min} = \sigma_v$. (d) An example of observed azimuthal variation from the eastern Snake River Plain.

elongate axis corresponds to the maximum or minimum compressive stress.

The contemporary state of stress in the Cordillera is extensional, with a possible component of strike-slip along the western margin of the Colorado Plateau [*Zoback and Zoback*, 1989; *Bjarnason and Pechmann*, 1989; *Smith and Arabasz*, 1991]. Minimum horizontal compressive stress directions from various stress indicators are given in Figure 8a. Minimum compressive stress has been interpreted to be approximately NE in the eastern Snake River Plain, E-W in the eastern Basin-Range and NNE-directed in the Colorado Plateau [*Zoback and Zoback*, 1989].

Given the extensional regime, minor axes of T_e anisotropy should correspond to the minimum horizontal compression direction. Vectors representing the minor axis direction of best fit T_e ellipses are scaled by elliptical eccentricity and plotted in Figure 8b. Stress directions inferred from T_e anisotropy are in close agreement with stress indicator data from the northeast Basin-Range, where $\sigma_{h\min}$ is ~E-W, and the eastern Snake River Plain, where NE directed $\sigma_{h\min}$ is observed. Interestingly, we do not observe significant anisotropy of T_e in the interior of the Basin-Range. In the Colorado Plateau, azimuthal variation of T_e suggests an ~ENE extension direction as compared to the NE to NNE extension direction inferred from earthquake focal mechanisms [*Wong and Humphrey*, 1989; *Zoback and Zoback*, 1989].

The largest strength anisotropy in the study area is observed near the Wasatch fault zone, Utah, where minimum T_e directions are orthogonal to the Wasatch fault in the hanging wall and parallel in the footwall. This apparent rotation of stress field is not well resolved by independent stress orientation data: several of the $\sigma_{h\min}$ directions indicated by fault slip and focal mechanisms on the Wasatch are consistent with the E-W minimum T_e direction west of the fault, but the only support for ~N-S $\sigma_{h\min}$ east of the fault comes from a ~500 m deep hydraulic fracture experiment. However, the rotation is consistent with contemporary horizontal strain. Trilateration measurements from 1972 to 1990 indicate N85°E uniaxial extension in the hanging wall block, and N20°E extension in the footwall block of the fault [*Savage et al.*, 1992]. The observed strength anisotropy is not a result of the extreme footwall flexure of the Wasatch [e.g., *Parry and Bruhn*, 1987], as the direction of reduced strength is orthogonal to that predicted for footwall bending.

There are places where stress directions and anisotropy of T_e are decidedly inconsistent; Yellowstone and its surroundings are an example. Focal mechanisms of the 1959 M_S 7.5 Hebgen Lake, Montana earthquake and its aftershocks suggest ~NNE extension, but T_e is lowest WNW. Inversion of Yellowstone earthquake focal mechanisms [*Peyton*, 1991] and Global Positioning Satellite measurements [*Meertens et al.*, 1993] likewise indicate NE extension. Strain behavior at

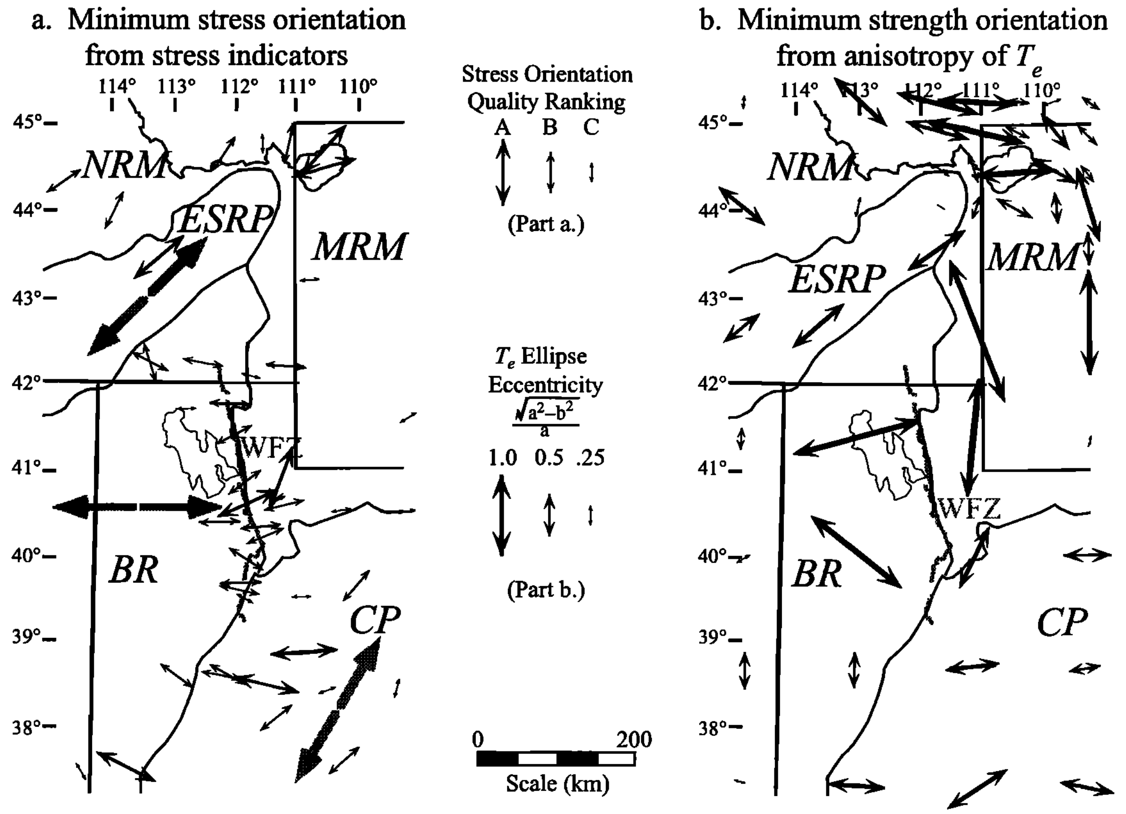

Figure 8. State of stress in the Basin-Range transition to the Colorado Plateau and Rocky Mountains. (a) Orientations of minimum horizontal compressive stress, from the compilation of *Zoback and Zoback* [1989]. (b) Minor axis directions of best fitting ellipses to polar plots of T_e.

Yellowstone is very heterogeneous with regard to both time and space [e.g., *Smith and Braile*, 1994], and so the discrepancy may be due to differences in the timescales and spatial wavelengths sampled by T_e versus stress indicators. Alternatively, it is possible that sensitivity of T_e to strain rate is amplified by rheological channeling of crustal flow in some regions. Our simplistic, one-dimensional model of T_e is insufficient to examine the latter possibility; a three-dimensional, dynamical model of lithospheric strength behavior would be required. Nevertheless, lithospheric state of stress appears to influence T_e throughout much of the Cordillera.

Earthquake Focal Depths

Many investigations associate focal depths of large, $M > 6$, earthquakes with the transition from frictional slip (brittle) to dislocation creep (ductile) deformation [e.g., *Sibson*, 1982; *Smith and Bruhn*, 1984] or a transition from velocity weakening (i.e., unstable) to velocity strengthening (i.e., stable) frictional slip behavior [e.g., *Tse and Rice*, 1986]. Velocity strengthening frictional slip and dislocation creep are end-members of a single continuum of deformation behavior, however [*Tse and Rice*, 1986], and each depends fundamentally on temperature and composition. Maximum focal depths of smaller, background seismicity may similarly depend on rheology, or they may depend instead on state of stress if stress is insufficient to fail the lithosphere near the rheological transition. The latter possibility seems unlikely in the ISB, however, where background seismic depths approach the focal depths of larger events. In any case, focal depths for both large and small earthquakes will depend on many of the same parameters as effective elastic thickness, and so we expect there should be a relationship between earthquake focii and T_e.

Unfortunately, observing that relationship is problematic. Maximum focal depths of background seismicity are not well constrained in the ISB because of poor sampling in both time and space. Focal depth information is available for only a small fraction of the earthquake cycle, and regional seismograph networks do not provide reliable depths for most smaller events except in special densified study areas [*Smith and Bruhn*, 1984; *Smith and Arabasz*, 1991]. In the ISB, focal depths of small events are considered reliable if the vertical hypocentral error calculated by the location algorithm is 2 km or less and the distance to the nearest seismometer is less than the focal depth [*Arabasz et al.*, 1990]. Seismograph spacing is ~35 km along the Wasatch Front, and ~20 km in the eastern Snake River Plain and Yellowstone [*Smith and Arabasz*, 1991; *Jackson et al.*, 1993; *Smith and Braile*, 1994]. Elsewhere, spacing is greater, typically exceeding 50 km. We carefully selected the most reliable focal depths from the ISB using the above criteria; these are plotted with T_e in Figures 9, 10, and 11. With the exceptions of the aftershock sequence for the 1983 M_L 7.3 Borah Peak, Idaho, earthquake (Figure 11a) and continuing activity near the 1959 M_S 7.5 Hebgen Lake, Montana, event (Figure 11b), maximum focal depths approximately coincide with T_e. It would be hazardous to assess a relationship when the data are spatially parameterized, however. Not only is the earthquake distribution poorly sampled, but T_e and earthquakes are sensitive to rheological properties at

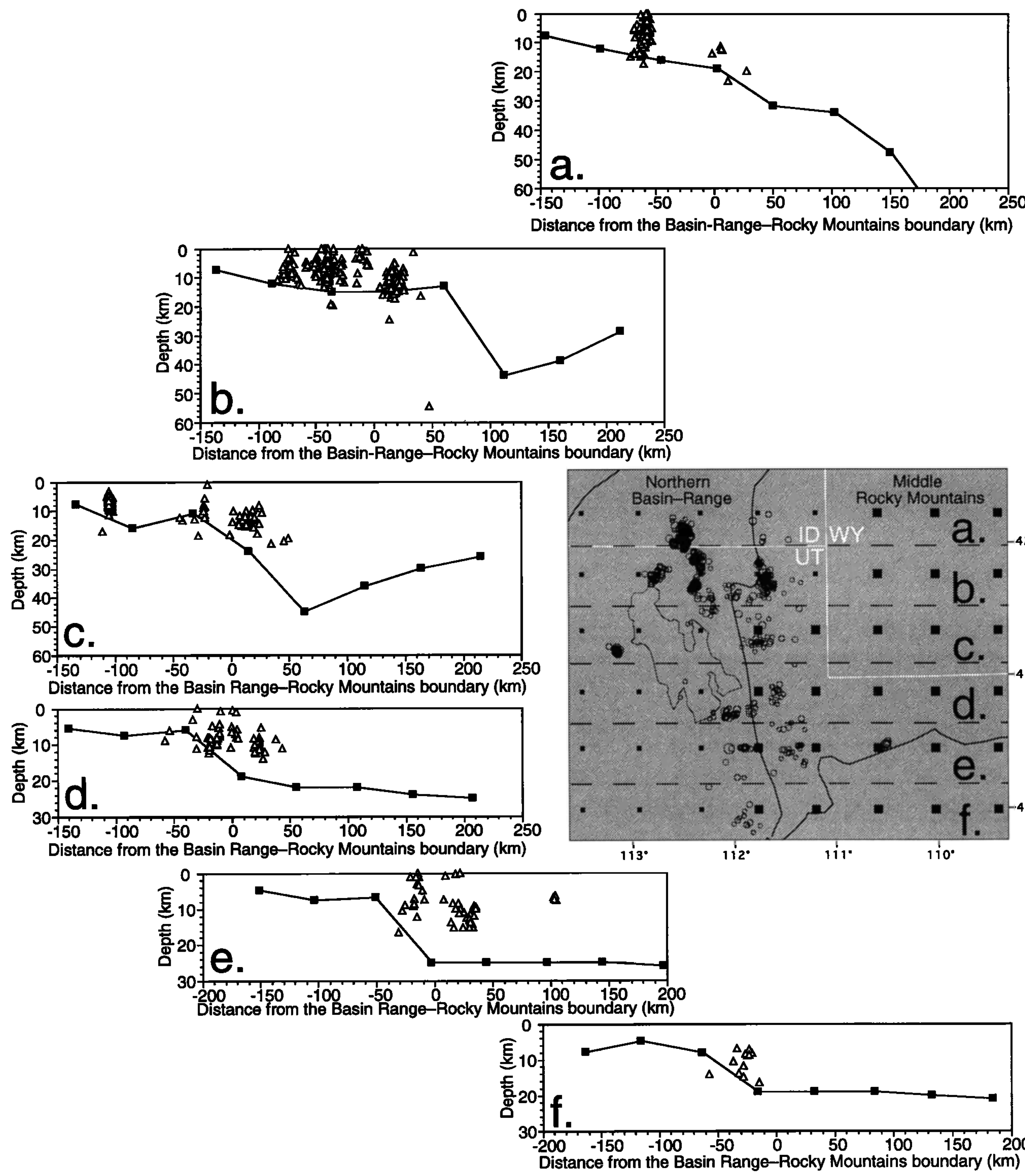

Figure 9. Focal depths plotted with T_e for the Basin-Range transition to the middle Rocky Mountains physiographic province. See Plate 1 for location of study area.

completely different spatial scales as well: whereas earthquakes respond to the physical state within a relatively small volume of rock, the absolute limit of resolution for T_e estimation occurs at wavelengths of ~40 km. Thus comparison of T_e and earthquake focal depth is liable to be valid only for gross statistical relationships.

Figure 12 shows focal depths plotted against T_e at the epicentral location, along with the predicted relationship of T_e to the depth of rheological transition from frictional to dislocation creep behavior. The latter relationship is insensitive to power law composition; relations for both dry granite and diorite are shown and are virtually indistinguishable. There are several notable relationships. The 95th percentile depth of background seismicity, calculated for 5-km-wide bins, approximately tracks T_e (as might have been deduced from previous figures). Regression of the depths of ISB background

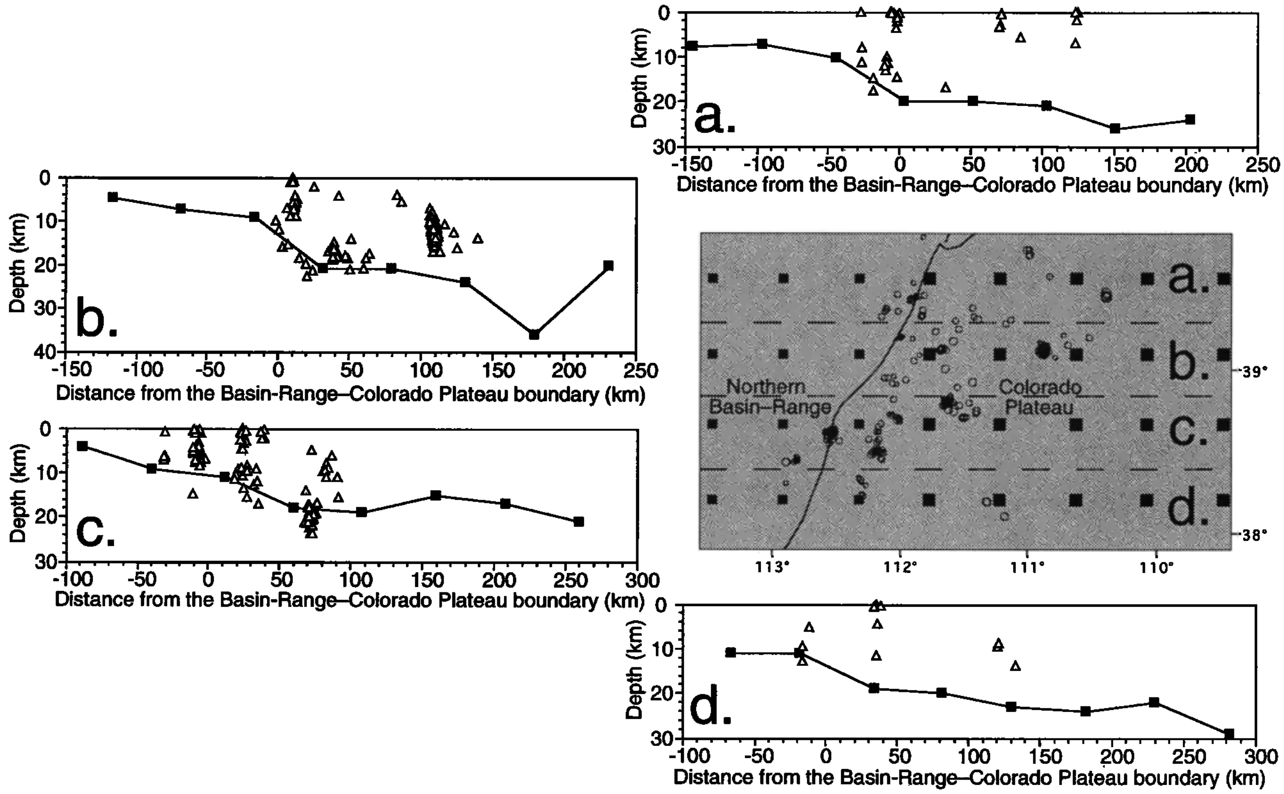

Figure 10. Focal depths plotted with T_e for the Basin-Range–Colorado Plateau transition. See Plate 1 for location of study area.

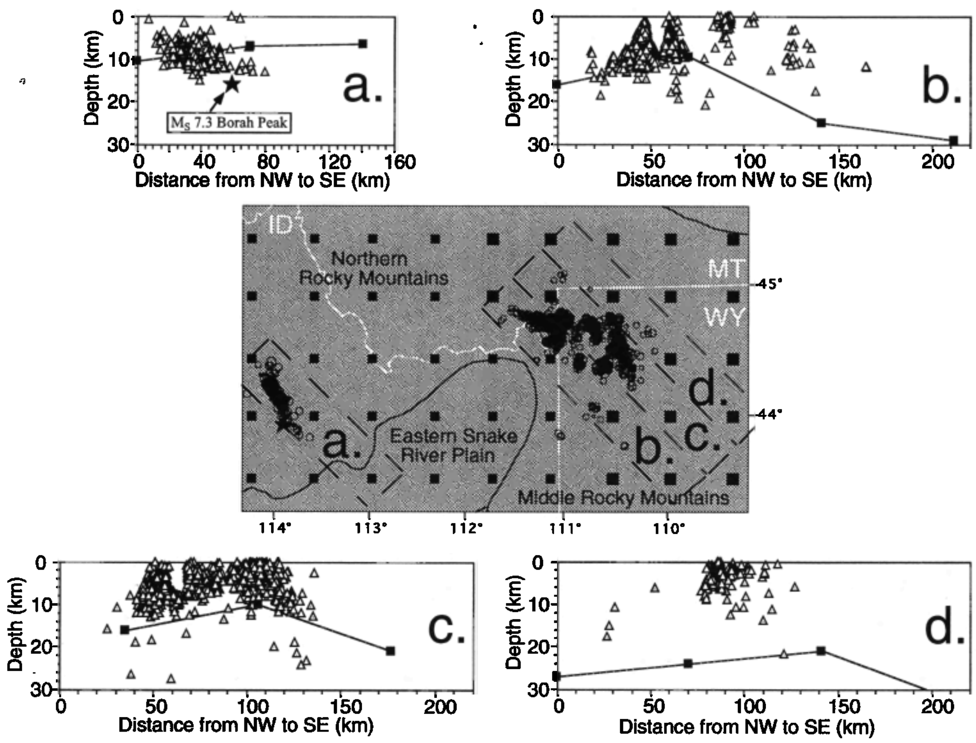

Figure 11. Focal depths plotted with T_e for (a) the Borah Peak aftershock sequence, (b) southwestern Yellowstone and Hebgen Lake, (c) central Yellowstone, and (d) northeastern Yellowstone. See Plate 1 for location of study area.

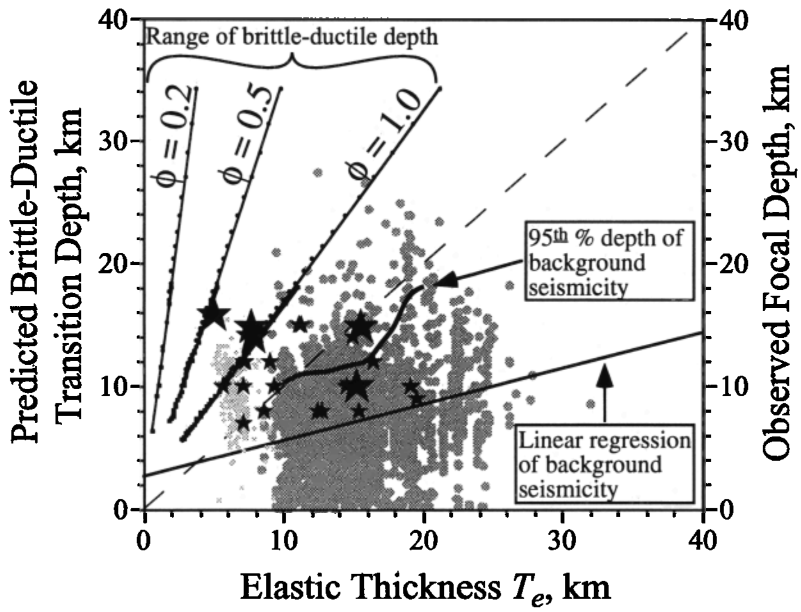

Figure 12. Focal depths of large earthquakes from the western U.S. Cordillera [after *Doser and Smith*, 1989], ISB background seismicity, and aftershocks of $M > 7$ events plotted as a function of effective elastic thickness. The relationship of T_e to brittle-ductile depth is also shown for a range of possible stress states $\phi = (\sigma_{h\max} - \sigma_{h\min})/(\sigma_v - \sigma_{h\min})$.

seismicity yields a positive correlation of depths to T_e to > 99.5% confidence, with correlation coefficient 0.3. That correlation suggests that maximum focal depth depends on some of the same parameters that define T_e.

Of the 5144 events shown, only a handful of the background earthquakes and a few of the very largest earthquakes (and their aftershocks) are deep enough to associate with brittle-ductile control, however. The deepest background earthquakes are almost certainly outliers, probably representing high-strength regions too small to be resolved by T_e estimation. Hence maximum focal depths of background seismicity are defined by some shallower rheological transition, most probably the stick-slip to stable sliding transition argued for by *Tse and Rice* [1986]. Enough of the large earthquakes fall into the range of possible brittle-ductile control to make the possibility somewhat harder to dismiss. Many studies have noted that some large mainshocks initiate at significantly greater depth than their aftershocks or nearby background activity. *Das* [1982] argued that the increase in strain rate during large earthquakes, approaching 10^{-4} to 10^{-3} s^{-1}, has the effect of deepening the brittle-ductile transition, but while that explains why ruptures might propagate to great depth, it does not explain why large events should initiate there. Instead, nucleation of large ruptures below the depth of regional-scale dislocation creep may result from stable slip heterogeneities induced by localized, compositionally defined strength variations along the fault plane. This hypothesis is also consistent with observations that large rupture events often nucleate in or near high velocity zones [e.g., *Lees and Malin*, 1990; *Lees and Nicholson*, 1993; *Foxall et al.*, 1993].

Other Implications of T_e

An important result of this analysis is that effective elastic thickness strongly depends on bulk composition of the rheological layers that compose the lithosphere. With careful consideration of complementary data sets, it should be possible to gather new clues regarding genesis of the lithosphere from mapped T_e (Plate 1a), even in areas where basement rocks are concealed by sedimentary or volcanic cover. The high T_e of the interior Columbia Basin is a good example (Plate 1a). Given the anomalously low heat flow (Figure 1) and proximity of Cascadia subduction, one could be tempted to interpret high strength as an artefact of thermal perturbation by cold subducting lithosphere. However, upper mantle *P* velocity indicates a steep eastward dip of the modern Juan de Fuca slab [*Humphreys and Dueker*, 1994], and modeling of Cenozoic subduction suggests negligible thermal perturbation east of central Washington state since 20 Ma [*Severinghaus and Atwater*, 1991]. The feature is near a known accretionary terrane, however: the Blue Mountains terrane, corresponding to lower strength regions to the south and east, derives from Paleozoic island arc volcanism [e.g., *White et al.*, 1992]. The Blue Mountains terrane is apparently a small exotic heralding a Precambrian terrane to the northwest, currently obscured by Columbia basalts. The postulated Precambrian origin is supported by high upper mantle *P* velocity to depths of 200 km [*Humphreys and Dueker*, 1994].

In another example, *Farmer and DePaolo* [1983] suggest that a discontinuity in the crustal contamination of granites (the dashed grey line (1) in Plate 1a) corresponds to the western edge of the Paleozoic craton, composed of lithosphere attenuated by latest Proterozoic rifting. However, the central Basin-Range is distinguished from lithosphere to the east by higher ε_{Sr} [*Farmer and DePaolo*, 1983], and T_e (Plate 1a) indicates distinct lithospheric blocks as opposed to a gradational decrease in strength between the Colorado Plateau and the central Basin-Range. The high ε_{Sr} isotopic domain also exhibits relative high topography and greater crustal thickness than the surrounding Basin-Range, and it is the Tertiary locus of an unextended belt sandwiched by large detachments to east and west [e.g., *Axen et al.*, 1993]. Hence we propose that older crustal material underlying the Paleozoic geoclinal sediments between lines (1) and (2) of Plate 1a is attached to pieces of exotic lithosphere, presumably terranes that accreted prior to the rifting event, that were then rafted away from the craton by early Paleozoic extension.

Also, a large area surrounding the active Yellowstone volcanic field indicates lower crustal flow rather than the mantle rheology typical of the remainder of the middle Rocky Mountains. A recent study by *Byrd et al.* [1994] indicates most of the 2 to 3 km offset on the Teton fault, 20 km south of Yellowstone, has occurred since ~2 Ma, coinciding with the approximate time of arrival of the Yellowstone hotspot [*Smith and Braile*, 1994]. This would imply that the source of the volcanism may also be responsible for mobilization of the lower crust, reduced T_e and the onset or acceleration of extension. However, this area also experienced effusive andesitic volcanism during the Laramide orogeny at ~50 Ma. Therefore, while thermal perturbation and mass flux associated with Yellowstone volcanism contribute to the current extensional episode, the lithosphere near Yellowstone probably was never as stable as cratonic lithosphere to the south and east.

T_e provides some insight into ISB extension as well. There is ample evidence that a significant fraction of Cordilleran tectonism is indirectly related to plate interactions, especially subduction processes [e.g., *Wernicke et al.*, 1987; *Severinghaus and Atwater*, 1990; *Axen et al.*, 1993]. Nevertheless the spatial relationships of Cordilleran extension and ISB seismicity to T_e (Plate 1) suggest strong control by other factors. Extensional strength of the lithosphere is controlled by the same parameters that determine T_e [e.g., *Kusznir and Park*, 1987], so the lithosphere should be weakest approximately where T_e is lowest. It is expected [e.g., *Chen and Molnar*, 1983] that much of the strain response to a uniform regional stress (such as an intraplate stress originating at a plate boundary) will be absorbed by the weakest portions of the lithosphere. However, there is relatively little seismic activity and contemporary strain where T_e is lowest: the main ISB seismicity (Plate 1a) is found instead in a zone of transition from low to high T_e. Hence the forces responsible for Cordilleran extension must originate locally, e.g., from nearby buoyancy distributions, rather than in the far field.

Zoback [1992] infers a local, buoyancy-related origin for extensional stresses from the relationship of topography to global distribution of stress. *Artyushkov* [1973] similarly suggests that the largest intraplate stresses are likely to result from lateral buoyancy variations, i.e., changes in the vertically integrated density column of the lithosphere. Much of the ISB (Plate 1a) corresponds to a major discontinuity in lithospheric buoyancy. Buoyancy variations alone are not enough to explain the seismicity however: if they were, seismicity would be equally vigorous at passive continental margins. The important difference is that crustal ductile behavior occurs throughout the ISB. Hence the concentration of seismicity in the ISB results from large stresses that are accommodated by flux of low-viscosity crustal material across buoyancy gradients [e.g., *Bird*, 1991].

Conclusions

T_e of the western U.S. Cordillera exhibits qualitative relationships to heat flow, lithospheric age, and Quaternary normal faulting. An improved understanding of these relationships is achieved by parameterization using a yield strength envelope. Comparisons with regional heat flow, seismically defined crustal properties, and principal stress orientations confirms that T_e is most sensitive to temperature, stress state, and composition at depths of ductile flow. Various tectonic provinces accommodate isostatic response at different levels of the crust or upper mantle, depending principally on the age of the lithosphere. T_e in the Archean middle Rocky Mountains is controlled primarily by ductile flow in the mantle. The Early Proterozoic-aged Colorado Plateau exhibits lower crustal control of long-term T_e. Latest Proterozoic-aged lithosphere that has experienced significant Cenozoic extension, including most of the Basin-Range, the various volcanic provinces (with the exception of the interior Columbia Basin), and the northern Rocky Mountains, accommodates flexure via middle to upper crustal ductile flow. Apparent lower crustal control of T_e in the interior Columbia Basin and the central Basin-Range likely corresponds to exotic terranes of older continental lithosphere.

Azimuthal variation of T_e exhibits a relationship to principal horizontal stress orientation. Anisotropy of T_e aligns with stress orientations inferred from stress indicators in the northeast Basin-Range, eastern Snake River Plain, and Colorado Plateau, but is less consistent with stress orientations from the very dynamic Yellowstone volcanic system. Azimuthal variation of T_e also implies an ~90° rotation of stress orientation across the Wasatch Front. Comparison of T_e with maximum earthquake focal depths indicates that background seismic depths are too shallow for control by the brittle-ductile transition, but some of the largest ($M > 7$) earthquakes and their aftershocks initiate within the range of possible brittle-ductile depths. Finally, qualitative relationships between T_e and the spatial distribution of seismicity and active faulting suggest that seismicity and tectonism in the Intermountain seismic belt are related more intimately to local buoyancy than to interactions at distant plate boundaries.

Acknowledgments. This manuscript was greatly improved by careful reviews by E. Humphreys, C. Lowe, and A. G. Jones. Animated discussions with J. O. D. Byrd, R. L. Bruhn, R. W. Simpson, and J. M. Bartley aided in crystallization of some of the ideas presented. We are deeply indebted to D. Forsyth and T. Bechtel for their development of the coherence method and to M. Zuber for providing access to Bechtel's original computer code. This study owes much to the dedicated work of the University of Utah Seismograph Stations crew, particularly W. Arabasz, J. C. Pechmann, and S. Nava. Pechmann also gave invaluable advice on the quality of earthquake hypocenter locations. Thanks also to D. Blackwell for providing the regional heat flow data, to M. L. Zoback for the stress orientation data, to J. Louie for the combined California-Nevada earthquake catalog, and to Rick Saltus for the USGS topography and Bouguer gravity gridded data sets. Support was provided by the National Science Foundation through grants EAR 89-04473 and EAR 92-19694.

References

Angelier, J., Tectonic analysis of fault slip data sets, *J. Geophys. Res.*, *89*, 5835–5848, 1984.

Arabasz, W. J., J. C. Pechmann, and E. D. Brown, Observational seismology and the evaluation of earthquake hazards and risk in the Wasatch Front area, Utah, *USGS Prof. Pap.*, *1500-D*, 1990.

Armin, R. A., and L. Mayer, Subsidence analysis of the Cordilleran miogeocline: Implications for timing of late Proterozoic rifting and amount of extension, *Geology*, *11*, 702–705, 1983.

Artyushkov, E. V., Stresses in the lithosphere caused by crustal thickness inhomogeneities, *J. Geophys. Res.*, *78*, 7675–7708, 1973.

Atwater, T., Implications of plate tectonics for Cenozoic tectonic evolution of western North America, *Geol. Soc. Am. Bull.*, *81*, 3513–3536, 1970.

Axen, G. J., W. J. Taylor, and J. M. Bartley, Space-time patterns and tectonic controls of Tertiary extension and magmatism in the Great Basin of the western United States, *Geol. Soc. Am. Bull.*, *105*, 57–76, 1993.

Bechtel, T. D., Mechanisms of isostatic compensation in East Africa and North America, Ph.D. dissertation, 247 pp., Brown Univ., Providence, R. I., 1989.

Bechtel, T. D., D. W. Forsyth, V. L. Sharpton, and R. F. Grieve, Variations in effective elastic thickness of the North American lithosphere, *Nature*, *343*, 636–638, 1990.

Benz, H. M., R. B. Smith, and W. D. Mooney, Crustal structure of the northwestern Basin-Range province from the 1986 Program for Array Seismic Studies of the Continental Lithosphere seismic experiment, *J. Geophys. Res.*, *95*, 21,823–21,842, 1990.

Bird, P., Lateral extrusion of lower crust from under high topography, in the isostatic limit, *J. Geophys. Res.*, *96*, 10,275–10,286, 1991.

Bird, P., and X. Kong, Computer simulations of California tectonics confirm low strength of major faults, *Geol. Soc. Am. Bull.*, *106*, 159–174, 1994.

Bjarnason, I. T., and J. C. Pechmann, Contemporary tectonics of the Wasatch Front region, Utah, from earthquake focal mechanisms, *Bull. Seismol. Soc. Am.*, *79*, 731–755, 1989.

Blackwell, D. D., and J. L. Steele, Geothermal map of North America, scale 1:5,000,000, Geol. Soc. of Am., Boulder, Colo., 1992.

Blackwell, D. D., J. L. Steele, and L. S. Carter, Heat-flow patterns of the North American continent: A discussion of the geothermal map of North America, in *Neotectonics of North America, Decade Map*, vol. 1, edited by D. B.Slemmons, E. R. Engdahl, M. D. Zoback, and D. D. Blackwell, pp. 423–436, Geological Society of America, Boulder, Colo., 1991.

Bond, G. C., and M. A. Kominz, Construction of tectonic subsidence curves for the early Paleozoic miogeocline, southern Canadian Rocky Mountains: Implications for subsidence mechanisms, age of breakup, and crustal thinning, *Geol. Soc. Am. Bull.*, *95*, 155–173, 1984.

Brace, W. F., and D. L. Kohlstedt, Limits on lithospheric stress imposed by laboratory experiments, *J. Geophys. Res.*, *85*, 6248–6252, 1980.

Braile, L. W., R. B. Smith, G. R. Keller, R. M. Welch, and R. P. Meyer, Crustal structure across the Wasatch Front from detailed seismic refraction studies, *J. Geophys. Res.*, *79*, 2669–2677, 1974.

Braile, L. W., R. B. Smith, J. Ansorge, M. R. Baker, M. A. Sparlin, C. Prodehl, M. M. Schilly, J. H. Healy, St. Mueller, and K. H. Olsen, The Yellowstone-Snake River Plain seismic profiling experiment: Crustal structure of the eastern Snake River Plain, *J. Geophys. Res.*, *87*, 2597–2609, 1982.

Braile, L. W., W. J. Hinze, R. R. B. von Frese, and G. R. Keller, Seismic properties of the crust and uppermost mantle of the conterminous United States and adjacent Canada, in Geophysical Framework of the Continental United States, edited by L. C. Pakiser and W. D. Mooney, *Geol. Soc. Am. Mem.*, *172*, 655–680, 1989.

Byrd, J. O. D., R. B. Smith, and J. W. Geissman, Neotectonics of the Teton fault, Wyoming, *J. Geophys. Res.*, *99*, 20,095–20,122, 1994.

Chen, W., and P. Molnar, Focal depths of intracontinental and intraplate earthquakes and their implications for the thermal and mechanical properties of the lithosphere, *J. Geophys. Res.*, *88*, 4183–4214, 1983.

Condie, K. C., *Archean Greenstone Belts*, Elsevier Scientific, New York, 1981.

Das, S., Appropriate boundary conditions for modeling very long earthquakes and physical consequences, *Bull. Seismol. Soc. Am.*, *72*, 1911–1926, 1982.

DeMets, C., R. G. Gordon, S. Stein, and D. F. Argus, A revised estimate of Pacific-North America motion and implications for western North America plate boundary zone tectonics, *Geophys. Res. Lett.*, *14*, 911–914, 1987.

DePaolo, D. J., Neodymium isotopes in the Colorado Front Range and crust formation and mantle evolution in the Proterozoic, *Nature*, *291*, 193–196, 1981.

Dixon, T. H., S. Robaudo, and J. Lee, Constraints on present day Basin and Range deformation from space geodesy, *Tectonics*, in press, 1995.

Doser, D. I., and R. B. Smith, An assessment of source parameters of earthquakes in the Cordillera of the western United States, *Bull. Seismol. Soc. Am.*, *79*, 1383–1409, 1989.

Dzurisin, D., J. C. Savage, and R. O. Fournier, Recent crustal subsidence at Yellowstone Caldera, Wyoming, *Bull. Volcanol.*, *52*, 247–270, 1990.

Eddington, P. K., R. B. Smith, and C. Renggli, Kinematics of Basin-Range intraplate extension, in Continental Extensional Tectonics, edited by M. P. Coward, J. F. Dewey, and P. L. Hancock, *Geol. Soc. Spec. Publ. London*, *28*, 371–392, 1987.

Farmer, G. L., and D. J. DePaolo, Origin of Mesozoic and Tertiary granite in the western United States and implications for pre-Mesozoic crustal structure, 1; Nd and Sr isotopic studies in the geocline of the northern Great Basin, *J. Geophys. Res.*, *88*, 3379–3401, 1983.

Fleck, R. J., and R. E. Criss, Strontium and oxygen isotopic variations in Mesozoic and Tertiary plutons of central Idaho, *Contrib. Mineral. Petrol.*, *90*, 291–308, 1985.

Forsyth, D. W., Finite extension and low-angle normal faulting, *Geology*, *20*, 27–30, 1992.

Fountain, D. M., and N. I. Christensen, Composition of the continental crust and upper mantle: A review, in Geophysical Framework of the Continental United States, edited by L. C. Pakiser and W. D. Mooney, *Geol. Soc. Am. Mem.*, *172*, 711–742, 1989.

Foxall, W., A. Michelini, and T. V. McEvilly, Earthquake travel time tomography of the southern Santa Cruz Mountains: Control of fault rupture by lithological heterogeneity of the San Andreas fault zone, *J. Geophys. Res.*, *98*, 17,691–17,710, 1993.

Gephart, J. W., and D. W. Forsyth, An improved method for determining the regional stress tensor using earthquake focal mechanism data: Application to the San Fernando earthquake sequence, *J. Geophys. Res.*, *89*, 9305–9320, 1984.

Goetze, C., and B. Evans, Stress and temperature in the bending lithosphere as constrained by experimental rock mechanics, *Geophys. J. R. Astron. Soc.*, *59*, 463–478, 1979.

Gough, D. I., and J. S. Bell, Stress orientations from oil well fractures in Alberta and Texas, *Can. J. Earth Sci.*, *18*, 638–645, 1981.

Hansen, F. D., and N. L. Carter, Creep of selected crustal rocks at 1000 MPa, *Eos Trans. AGU*, *63*, 437, 1982.

Hecker, S., Quaternary tectonics of Utah with emphasis on earthquake-hazard characterization, *Utah Geol. Surv. Bull.*, *127*, 157 pp., 1993.

Hickman, S. H., and M. D. Zoback, The interpretation of hydraulic fracturing process-time data for in situ stress determination, in *Hydraulic Fracturing Stress Measurements*, edited by M. D. Zoback and B. C. Haimson, pp. 44–54, National Academy Press, Washington, D.C., 1983.

Hill, D. P., and L. C. Pakiser, Crustal structure between the Nevada Test Site and Boise, Idaho, from seismic refraction measurements, in *The Earth Beneath the Continents*, *Geophys. Monogr. Ser.*, vol. 10, edited by J. S. Steinhart and T. J. Smith, pp. 391–419, AGU, Washington, D. C., 1966.

Humphreys, E. D., and K. G. Dueker, Western U.S. upper mantle structure, *J. Geophys. Res.*, *99*, 9615–9634, 1994.

Jackson, S. M., I. G. Wong, G. S. Carpenter, D. M. Anderson, and S. M. Martin, Contemporary seismicity in the eastern Snake River Plain, Idaho, based on microearthquake monitoring, *Bull. Seismol. Soc. Am.*, *83*, 680–695, 1993.

Jordan, T. H., Composition and development of the continental tectosphere, *Nature*, *274*, 544–548, 1978.

Jordan, T. H., Continents as a chemical boundary layer, *Philos. Trans. R. Soc. London A*, *301*, 359–373, 1981.

Kirby, S. H., Rheology of the lithosphere, *Rev. Geophys.*, *21*, 1458–1487, 1983.

Kusznir, N. J., and R. J. Park, The extensional strength of the continental lithosphere: Its dependence on geothermal gradient, and composition and thickness, in Continental Extensional Tectonics, edited by M. P. Coward, J. F. Dewey and P. L Hancock, *Geol. Soc. Spec. Publ. London, 28*, 22–52, 1987.

Leeman, W. P., J. S. Oldow, and W. K. Hart, Lithosphere-scale thrusting in the western U. S. Cordillera as constrained by Sr and Nd isotopic transitions in Neogene volcanic rocks, *Geology, 20*, 63–66, 1992.

Lees, J. M., and P. E. Malin, Tomographic images of *P* wave velocity variation at Parkfield, California, *J. Geophys. Res., 95*, 21,793–21,804, 1990.

Lees, J. M., and C. Nicholson, Three-dimensional tomography of the 1992 southern California earthquake sequence: Constraints on dynamic earthquake rupture? *Geology, 21*, 387–390, 1993.

Lehman, J. A., R. B. Smith, M. M. Schilly, and L. W. Braile, Upper crustal structure of the Yellowstone caldera from delay time analyses and gravity correlations, *J. Geophys. Res., 87*, 2713–2730, 1982.

Lowry, A. R., and R. B. Smith, Flexural rigidity of the Basin-Range–Colorado Plateau–Rocky Mountain transition from coherence analysis of gravity and topography, *J. Geophys. Res., 99*, 20,123–20,140, 1994.

Lyon-Caen, H., and P. Molnar, Constraints on the structure of the Himalaya from an analysis of gravity anomalies and a flexural model of the lithosphere, *J. Geophys. Res., 88*, 8171–8192, 1983.

Manduca, C. A., L. T. Silver, and H. P. Taylor, $^{87}Sr/^{86}Sr$ and $^{18}O/^{16}O$ isotopic systematics and geochemistry of granitoid plutons across a steeply-dipping boundary between contrasting lithospheric blocks in western Idaho, *Contrib. Mineral. Petrol., 109*, 355–372, 1992.

Martinez, L. J., C. M. Meertens, and R. B. Smith, GPS surveys of the Wasatch fault zone, Utah, *Eos Trans. AGU, 75*(44), Fall Meeting suppl., 179–180, 1994.

McCamy, K., and R. P. Meyer, A correlation method of apparent velocity measurement, *J. Geophys. Res., 69*, 691–699, 1964.

McGarr, A., and N. C. Gay, State of stress in the earth's crust, *Annu. Rev. Earth Planet. Sci., 6*, 405–436, 1978.

McNutt, M. K., Lithospheric flexure and thermal anomalies, *J. Geophys. Res., 89*, 11,180–11,194, 1984.

McNutt, M. K., and H. W. Menard, Constraints on yield strength in the oceanic lithosphere derived from observations of flexure, *Geophys. J., 71*, 363–394, 1982.

Meertens, C. M., R. B. Smith, and D. W. Vasco, Kinematics of crustal deformation of the Yellowstone hotspot using GPS, *Eos Trans. AGU, 74*(43), Fall Meeting suppl., 63, 1993.

Minster, J. B., and T. H. Jordan, Vector constraints on western U. S. deformation from space geodesy, neotectonics, and plate motions, *J. Geophys. Res., 92*, 4798–4804, 1987.

Mueller, S., and M. Landisman, An example of the unified method of interpretation for crustal seismic data, *Geophys. J. R. Astron. Soc., 23*, 365–371, 1971.

Nakamura, K. K., Volcanoes as possible indicators of tectonic stress orientation– principle and proposal, *J. Volcanol. Geotherm. Res., 2*, 1–16, 1977.

O'Hara, N. W., and P. L. Lyons, New map updates gravity data, *Geotimes, 28*, 22–27, 1983.

Parry, W. T., and R. L. Bruhn, Fluid inclusion evidence for minimum 11 km vertical offset on the Wasatch Fault, Utah, *Geology, 15*, 67–70, 1987.

Peyton, S. L., Contemporary tectonics of the Yellowstone-Hebgen Lake region from earthquake focal mechanisms and stress field inversion, M.S. thesis, 90 pp., Univ. of Utah, Salt Lake City, 1991.

Roller, J. C., Crustal structure in the eastern Colorado Plateaus province from seismic-refraction measurements, *Bull. Seismol. Soc. Am., 55*, 107–119, 1965.

Savage, J. C., M. Lisowski, and W. H. Prescott, Strain accumulation across the Wasatch fault near Ogden, Utah, *J. Geophys. Res., 97*, 2071–2083, 1992.

Severinghaus, J., and T. Atwater, Cenozoic geometry and thermal state of the subducting slabs beneath western North America, in Basin-Range Extensional Tectonics Near the Latitude of Las Vegas, Nevada, edited by B. P. Wernicke, *Mem. Geol. Soc. Am., 176*, 1–22, 1990.

Sheriff, S. D., and M. C. Stickney, Crustal structure of southwestern Montana and east-central Idaho: Results of a reversed seismic refraction line, *Geophys. Res. Lett., 11*, 299–302, 1984.

Sibson, R. H., Frictional constraints on thrust, wrench and normal faults, *Nature, 249*, 542–544, 1974.

Sibson, R. H., Fault zone models, heat flow, and the depth distribution of earthquakes in the continental crust of the United States, *Bull. Seismol. Soc. Am., 72*, 151–163, 1982.

Simpson, R. W., R. C. Jachens, R. J. Blakely, and R. W. Saltus, A new isostatic residual map of the conterminous United States with a discussion on the significance of isostatic residual anomalies, *J. Geophys. Res., 91*, 8348–8372, 1986.

Smith, R. B., and W. J. Arabasz, Seismicity of the Intermountain seismic belt, in *Neotectonics of North America, Decade Map*, vol. 1, edited by D. B. Slemmons, E. R. Engdahl, M. D. Zoback, and D. D. Blackwell, pp. 185–228, Geological Society of America, Boulder, Colo., 1991.

Smith, R. B., and L. W. Braile, The Yellowstone hotspot, *J. Volcan. Geotherm. Res., 61*, 121–188, 1994.

Smith, R. B., and R. L. Bruhn, Intraplate extensional tectonics of the eastern Basin-Range: Inferences on structural style from seismic reflection data, regional tectonics, and thermal-mechanical models of brittle-ductile deformation, *J. Geophys. Res., 89*, 5733–5762, 1984.

Smith, R. B., and M. L. Sbar, Contemporary tectonics and seismicity of the western United States with emphasis on the Intermountain seismic belt, *Geol. Soc. Am. Bull., 85*, 1205–1218, 1974.

Sparlin, M. A., L. W. Braile, and R. B. Smith, Crustal structure of the eastern Snake River Plain determined from ray-trace modeling of seismic refraction data, *J. Geophys. Res., 87*, 2619–2633, 1982.

Tse, S. T., and J. R. Rice, Crustal earthquake instability in relation to the depth variation of frictional slip properties, *J. Geophys. Res., 91*, 9452–9472, 1986.

Turcotte, D. L., and G. Schubert, *Geodynamics: Applications of Continuum Physics to Geological Problems*, John Wiley, New York, 1982.

Wernicke, B. P., Cenozoic extensional tectonics of the U. S. Cordillera, in *The Cordilleran Orogen: Conterminous U.S., Geol. of N. Am.*, vol. G-3, edited by B. C. Burchfiel, P. W. Lipman, and M. L. Zoback, pp. 553–581, Geological Society of America, Boulder, Colo., 1991.

Wernicke, B. P., R. L. Christiansen, P. C. England, and L. J. Sonder, Tectonomagmatic evolution of Cenozoic extension in the North American Cordillera, in Continental Extensional Tectonics, edited by M. P. Coward, J. F. Dewey, and P. L. Hancock, *Geol. Soc. Spec. Publ. London, 28*, 203–221, 1987.

White, J. D. L., D. L. White, T. Vallier, G. D. Stanley, and S. R. Ash, Middle Jurassic strata link Wallowa, Olds Ferry, and Izee terranes in the accreted Blue Mountains island arc, northeastern Oregon, *Geology, 20*, 729–732, 1992.

Wong, I. G., and J. R. Humphrey, Contemporary seismicity, faulting, and the state of stress in the Colorado Plateau, *Geol. Soc. Am. Bull., 101*, 1127–1146, 1989.

Zoback, M. L., First- and second-order patterns of stress in the lithosphere: The world stress map project, *J. Geophys. Res., 97*, 11,703–11,728, 1992.

Zoback, M. L., and M. D. Zoback, Tectonic stress field of the continental United States, in Geophysical Framework of the Continental United States, edited by L. C. Pakiser and W. D. Mooney, *Mem. Geol. Soc. Am., 172*, 523–539, 1989.

Zoback, M. D., et al., State of stress in the San Andreas fault system, *Science, 238*, 1105–1111, 1987.

A. R. Lowry and R. B. Smith, Department of Geology and Geophysics, College of Mines and Earth Sciences, University of Utah, Salt Lake City, UT 84112-1183. (e-mail: arlowry@mines.utah.edu)

(Received September 2, 1994; revised February 21, 1995;
accepted February 28, 1995.)